CO-ROTATIONAL FORMULATION AND IMPLEMENTATION OF AN INVARIANT-BASED MODEL FOR GEOMETRICALLY NONLINEAR ANALYSES OF COMPOSITES

Aamir Dean[1]and Raimund Rolfes[2]

[1&2] Institute of Structural Analysis, Leibniz Universität Hannover

a.dean@isd.uni-hannover.de r.rolfes@isd.uni-hannover.de

مُسْتَخْلَص

في هذه الورقة، في إطار الدوران المشترك (Co-rotational)، يتم صياغة وتنفيذ نموذج لدونة (Plasticity) غير متغير (Anisotropic) متباين الخواص (Invariant-based) ليستخدم في التحليل الهندسي الغير الخطي لمركبات البوليمرات المقواة بالألياف (FRP). تصاغ المعادلات التأسيسية (Constitutive equations) متباينة الخواص في شكل دوال الموترات متسقة الاتجاهات (Isotropic tensor functions). يعتمد النموذج على دالة خضوع (Yield function) متابينة الخواص والمعتمدة على الضغط، وبالإضافة إلى ذلك، تستخدم دالة جهد لدن غير مرتبطه (Non-associative plastic potential) من أجل توصيف تشوهات لدونة أكثر واقعية فيما يخص مركبات البوليمرات المقواة بالألياف. و من ثم، توضع الصياغة في إطار الدوران المشترك ويتم تنفيذها في برنامج العناصر المحدودة ابكوس (Abaqus/Standard) عبر البرنامج الفرعي الذي يتم تعرفيه من قبل المستخدم و المسمى يومات (UMAT). يتم وصف كينامتيكية التشوه المتناهي (Finite deformation kinematics) ضمن إطار الدوران المشترك و تناقش الجوانب الهامة المتعلقة بالمعالجة العددية والتنفيذ. اخيرا، يقيم أداء النموذج من خلال مجموعة من الامثلة العددية، والتي تبين متانة و قابلية تطبيق النموذج.

ABSTRACT

A co-rotational formulation and implementation of an invariant-based anisotropic plasticity model is presented for geometrically nonlinear analyses of Fiber Reinforced Polymer (FRP) composites. The anisotropic constitutive equations are formulated in the format of isotropic tensors functions. The model assumes an anisotropic pressure dependent yield function, and in addition to this, a non-associated plastic potential in order to model more realistic plastic deformations in FRP. The formulation is then cast in the co-rotational framework and implemented in the commercial finite element software Abaqus/Standard via the means of the user-defined capability UMAT. The finite deformation kinematics within the co-rotational frame are described and the important aspects regarding the numerical treatment and implementation are discussed. The performance of the model is assessed via a set of numerical simulations, which demonstrate its applicability and robustness.

Keywords: *FRP composites; Anisotropic plasticity; Co-rotational framework; FEM*

1 Introduction

In different engineering applications, the recent advent of new composites is promoting the replacement of traditionally employed materials. In various engineering applications, the recent development of innovative composites is promoting the substitute of traditionally utilized materials. In construction sector, Fiber Reinforced Polymer (FRP) composites are getting a substantial attractiveness mainly because of their flexibility, high strength-to-weight ratio, more rapid construction, increased durability and resistance to fatigue and corrosion, and lower routine maintenance and life-cycle costs [1]. However, when it comes to modeling and simulation these materials still pose a challenge. Because they exhibit rate-, temperature-, and pressure dependent as well as anisotropic material behavior and undergo large deformations during loading processes.

In order to accurately determine the correct stress state in composites, as well as to evaluate its strengths, by the means of structural simulation via FEA, Fiber orientation (anisotropy) is a substantial parameter. In this respect, there exist two primary different strategies to consider and to model the anisotropiy in FRP composites: (i) multiscale approaches (FE2 techniques), and (ii) macroscopic phenomenological strategies.

In [2], a thorough review on the multiscale modeling of composites is presented. However, as was amply discussed in the literature, one among the essential disadvantages of those multiscale techniques is the dramatic increase of the computational effort [3]. Consequently, in order to model the micro-structures of materials in practical engineering applications, the employment of multiscale techniques can be considered as rather limited and unpractical.

Differing from the previous set of techniques, fiber orientation is accounted for by using anisotropic macroscopic phenomenological material models. In this approach, experiments are used to acquire the homogenized macroscopic material properties. In the literature, there exist a fair number of works devoted for phenomenological modeling of FRP composites.

In general, the incorporation of anisotropy into macroscopic models can be carried out in different ways. A possible framework can be set up based on the invariant theory. Accordingly, anisotropic constitutive equations are represented in the format of isotropic tensor functions in terms of several tensor variables; kinematic or kinetic tensors, as well as additional structural tensors that represent the symmetries of the material under consideration. In [4], an extensive review of the recent developments in the theory, as well as numerical treatment of anisotropic materials, is given.

In this contribution, an invariant-based anisotropic plasticity model is formulated and implemented within the co-rotational framework for it's used in geometrically nonlinear analyses of FRP composites. In practical terms, the anisotropic constitutive equations are represented in the format of isotropic tensors functions. From the modeling viewpoint, anisotropic yield surfaces and non-associative plastic potential functions are introduced to regard the nonlinear inelastic behavior of these materials, see [5]. Non-associated plastic potential functions are introduced in order to model more realistic plastic deformations in FRP composites. The model is then cast in a co-rotational framework so that finite deformation responses can be simulated, wherein displacements and rotations are assumed finite while strains are assumed to be within the small (not exactly the small strain of linear deformation theory) to moderate rate [6]. From the computational standpoint, aspects concerning the corresponding algorithmic treatment of the proposed models, as well as the numerical implementation, are looked over. In particular, novel closed-form expressions necessary for the consistent finite element are derived. To assess the performance of the proposed model, a set of numerical simulations using the commercial finite element software Abaqus/Standard are presented.

2 Kinematics in the Co-rotational Framework

This section is devoted to the finite deformation kinematics within the co-rotational frame. For further details, the reader may refer to [6].

Assume a continuum body $\boldsymbol{\mathcal{B}}$ that is composed of infinitely many material points $P \in \boldsymbol{\mathcal{B}}$. The placement χ_t maps the material points $P \in \boldsymbol{\mathcal{B}}$ to a subset of the Euclidean space $\mathbb{R}^3$. At the initial time t_0 the body $\boldsymbol{\mathcal{B}}$ occupies the reference placement $\boldsymbol{\mathcal{B}}_0 \equiv \chi_{t_0}(\boldsymbol{\mathcal{B}}) \subset \mathbb{R}^3$ and material points $\mathbf{X} \coloneqq \chi_{t_0}(P) \in \boldsymbol{\mathcal{B}}_0$. As customary, the reference configuration is assumed to be undistorted stress-free. Subsequently, the corresponding current position of the continuum body is identified by $\boldsymbol{\mathcal{B}}_t \equiv \chi_t(\boldsymbol{\mathcal{B}}) \subset \mathbb{R}^3$, while the current position vector of an arbitrary point is denoted by $\mathbf{x} \coloneqq \chi_t(P) \in \boldsymbol{\mathcal{B}}_t$. The reference and the current configurations are related via the nonlinear deformation map $\varphi: \boldsymbol{\mathcal{B}}_0 \times [0,t] \longrightarrow \mathbb{R}^3$, where $[0,t]$ denotes the time interval elapsed such that the reference material points ($\mathbf{X} \in \boldsymbol{\mathcal{B}}_0$) are mapped onto the current material points ($\mathbf{x} \in \boldsymbol{\mathcal{B}}_t$), i.e. $\mathbf{x} = \varphi(\mathbf{X}, t)$. Accordingly, one defines the standard displacement vector as: $\mathbf{u} \coloneqq \mathbf{x} - \mathbf{X}$. The incremental mapping from $\boldsymbol{\mathcal{B}}_n$ to $\boldsymbol{\mathcal{B}}_{n+1}$ is denote by $\bar{\varphi}(\mathbf{x}, t)$.

The so-called deformation gradient $\mathbf{F}$ is expressed as $\mathbf{F}(\mathbf{X}, t) = \partial\varphi(\mathbf{X}, \mathrm{t})/\partial\mathbf{X} = \mathbf{1} + \nabla\mathbf{u}$, where $\mathbf{1}$ refers to the second-order identity tensor. Similarly, the incremental deformation gradient $\bar{\mathbf{F}}$ between $\boldsymbol{\mathcal{B}}_n$ and $\boldsymbol{\mathcal{B}}_{n+1}$ is given by $\bar{\mathbf{F}}_{n+1} = \partial\mathbf{x}_{n+1}/\partial\mathbf{x}_n = \mathbf{1} + \nabla\bar{\mathbf{u}}_{n+1}$.

Now, another mapping $\tilde{\varphi}(\mathbf{x}, t)$ that corresponds to the rotation of the body from $\boldsymbol{\mathcal{B}}_n$ to $\widetilde{\boldsymbol{\mathcal{B}}}_n$ is introduced. This mapping describes the body in the rotated frame so that $\tilde{\mathbf{x}} = \tilde{\varphi}(\mathbf{x}, t)$. Accordingly, the deformation gradient $\tilde{\mathbf{F}}$ between $\boldsymbol{\mathcal{B}}_n$ and $\widetilde{\boldsymbol{\mathcal{B}}}_n$ is given by $\tilde{\mathbf{F}}(\mathbf{X}, t) = \partial\tilde{\varphi}(\mathbf{x}, \mathrm{t})/\partial\mathbf{x}$. The previous relation leads to the definition of the

orthonormal co-rotational tensor which is denoted as **R**. Similarly, the incremental deformation gradient $\tilde{\bar{\mathbf{F}}}$ between $\widetilde{\boldsymbol{\mathcal{B}}}_n$ and $\widetilde{\boldsymbol{\mathcal{B}}}_{n+1}$ is given by $\tilde{\bar{\mathbf{F}}}_{n+1} = \partial\tilde{\mathbf{x}}_{n+1}/\partial\tilde{\mathbf{x}}_n = \mathbf{1} + \nabla\tilde{\bar{\mathbf{u}}}_{n+1}$. The tensor **R** is computed in the computational setting for each element in the discretized domain based on the co-rotational procedure, see [6].

Figure 1, schematically depicts the referential, spatial and co-rotational domain of the continuum body $\boldsymbol{\mathcal{B}}$.

Following the co-rotational formulation procedure, an arbitrary motion of the continuum body $\boldsymbol{\mathcal{B}}$ is assumed to be decomposed into a rigid body motion, superimposed

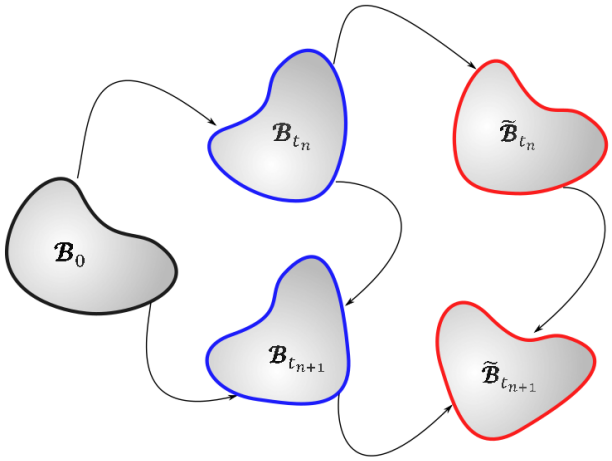

by a pure relative deformation [6].

Figure 1: Schematic representation of the referential (black), spatial (blue) and co-rotational frame (red).

In such case, the pure deformation part of the displacement field tends to be small when the incremental motion is sufficiently small. Based on this argument, in the rotated frame, the magnitude of calculated strains is of the order of small strains.

In the FE spatially discretized domain, the proposed decomposition can be achieved for each element by defining a local co-rotational coordinate frame that does not deform, but it rotates and translates with the element. After having on hand the pure deformation part of the displacement field, the strain is then computed with respect to this local frame. In this frame, the discrete gradients of the pure deformational field are small, so also the strain as compared to the element dimension. This is the main idea that is used to simplify the updated Lagranian formulation to the co-rotational formulation.

3 Constitutive Formulation

This section presents the constitutive formulation of the anisotropic invariant-based model for FRP composites. Note that, the constitutive equations are formulated with respect to the co-rotational frame $\widetilde{\boldsymbol{\mathcal{B}}}_n$. However, for notational simplicity, explicit indication $(\tilde{*})$ is being omitted.

From the modeling standpoint, the mechanical response admits a tensor-based representation through the definition of a second order structural tensor in the rotated frame **A**, which is defined as:

$$\mathbf{A} \coloneqq \mathbf{a}\otimes\mathbf{a} \quad (1)$$

where **a** identifies the fiber orientation vector in the rotated frame.

Based on the flow theory of plasticity, the total strain tensor $\boldsymbol{\varepsilon}$ is assumed to be additively split into elastic $\boldsymbol{\varepsilon}^e$ and plastic $\boldsymbol{\varepsilon}^p$ counterparts:

$$\boldsymbol{\varepsilon} = \boldsymbol{\varepsilon}^e + \boldsymbol{\varepsilon}^p \quad (2)$$

3.1 Transversely Isotropic Free Energy Definition

To formulate the constitute equations, the existence of a Helmholtz free energy function, $\psi(\boldsymbol{\varepsilon}^e, \mathbf{A}, \boldsymbol{\alpha})$ is assumed. This free energy is a function of the elastic strain $\boldsymbol{\varepsilon}^e$ and the structural tensor **A** in the in the rotated frame, and the internal variable set $\boldsymbol{\alpha}$ that accounts for the inelastic material response along the deformation process:

$$\psi(\boldsymbol{\varepsilon}^e, \mathbf{A}, \boldsymbol{\xi}) = \frac{1}{2}\boldsymbol{\varepsilon}^e : \mathbb{C} : \boldsymbol{\varepsilon}^e + \psi^{hard}(\boldsymbol{\xi}) \quad (3)$$

Where $\psi^{hard}(\boldsymbol{\xi})$ accounts for the hardening part of the free-energy function.

The Cauchy stress tensor $\boldsymbol{\sigma}$ and the elastic constitutive operator $\mathbb{C}$ are defined as the first and the second derivative of the free energy with respect to elastic strain tensor, respectively:

$$\boldsymbol{\sigma} \coloneqq \partial\psi/\partial\boldsymbol{\varepsilon}^e \; ; \; \mathbb{C} \coloneqq \partial^2\psi/\partial\boldsymbol{\varepsilon}^e\partial\boldsymbol{\varepsilon}^e \quad (4)$$

For transversely isotropic materials, the elasticity operator adopts the form:

$$\mathbb{C} \coloneqq \partial^2\psi/\partial\boldsymbol{\varepsilon}^e\partial\boldsymbol{\varepsilon}^e = \lambda\mathbf{1}\otimes\mathbf{1} + 2\mu_1\mathbf{I} + \alpha(\mathbf{1}\otimes\mathbf{A} + \mathbf{A}\otimes\mathbf{1}) + 2(\mu_2 - \mu_1)\mathbf{I}_\mathbf{A} + \beta\mathbf{A}\otimes\mathbf{A} \quad (5)$$

where **I** refers to the fourth-order identity tensor, whereas $\mathbf{I}_\mathbf{A} = \mathbf{A}_{im}\mathbf{I}_{jmkl} + \mathbf{A}_{jm}\mathbf{I}_{mikl}$, and λ, μ_1, μ_2, α, β denote the elastic constants.

3.2 The Clausius-Plank Inequality

The so-called Clausius-Plank inequality for internal dissipation $\mathcal{D}_{int}$ takes the form:

$$\mathcal{D}_{int} = \boldsymbol{\sigma} : \dot{\boldsymbol{\varepsilon}} - \dot{\psi} \geq 0 \quad (6)$$

Complying with the standard Truesdell and Noll procedure and recalling the previous definition given in Eq. (6), the following constitutive equations arise from Eq. (3):

$$\boldsymbol{\sigma} \coloneqq \partial\psi/\partial\boldsymbol{\varepsilon}^e = \mathbb{C} : \boldsymbol{\varepsilon}^e \quad (7)$$

$$\boldsymbol{\Gamma} \coloneqq -\partial\psi/\partial\boldsymbol{\xi} = -\partial\psi^{hard}/\partial\boldsymbol{\xi} \quad (8)$$

where $\boldsymbol{\Gamma}$ denotes the so-called hardening force.

With the previous definitions at hand, incorporating Eqs. (7) and (8), the restriction over the internal dissipation to fulfill the second law of the thermodynamics reads:

$$\mathcal{D}_{int} = \boldsymbol{\sigma} : \dot{\boldsymbol{\varepsilon}}^p - \boldsymbol{\Gamma} * \dot{\boldsymbol{\xi}} \geq 0 \quad (9)$$

where the operator $*$ stands for any arbitrary product.

3.3 Yield and Plastic Potential Functions

The elastic domain $\mathbb{E}$, assuming the maximum dissipation principle, can be defined as:

$$\mathbb{E} = \{(\boldsymbol{\xi}, \bar{\boldsymbol{\varepsilon}}^p) | \mathcal{F}(\boldsymbol{\sigma}, \mathbf{A}, \bar{\boldsymbol{\varepsilon}}^p) \leq 0\} \quad (10)$$

where $\bar{\boldsymbol{\varepsilon}}^p$ refers to the so-called equivalent plastic strain. The equivalent plastic strain in the current formulation is defined by:

$$\bar{\boldsymbol{\varepsilon}}^p := \sqrt{\frac{1}{2}\|\boldsymbol{\varepsilon}^p\|} = \sqrt{\frac{1}{2}\boldsymbol{\varepsilon}^p : \boldsymbol{\varepsilon}^p} \quad (11)$$

A transversely isotropic yield surface $\mathcal{F}(\boldsymbol{\sigma}, \mathbf{A}, \bar{\boldsymbol{\varepsilon}}^p)$ that accounts for the pressure dependency and plastic inextensibility of endless FRP composites along the fiber direction is constructed as follows:

$$\mathcal{F}(\boldsymbol{\sigma}, \mathbf{A}, \bar{\boldsymbol{\varepsilon}}^p) = \varsigma_1 I_1 + \varsigma_2 I_2 + \varsigma_3 I_3 + \varsigma_4 {I_3}^2 \leq 0 \quad (12)$$

$I_i (i = 1,3)$ identifies the stress invariants, which are defined as:

$$I_1 = (\mathrm{Tr}[\boldsymbol{\sigma} \cdot \boldsymbol{\sigma}] + (\mathrm{Tr}[\mathbf{A} \cdot \boldsymbol{\sigma}])^2 - 2\mathrm{Tr}[\mathbf{A} \cdot \boldsymbol{\sigma} \cdot \boldsymbol{\sigma}] - (\mathrm{Tr}[\boldsymbol{\sigma}] - \mathrm{Tr}[\mathbf{A} \cdot \boldsymbol{\sigma}])^2)/2 \quad (13)$$

$$I_2 = \mathrm{Tr}[\mathbf{A} \cdot \boldsymbol{\sigma} \cdot \boldsymbol{\sigma}] - (\mathrm{Tr}[\mathbf{A} \cdot \boldsymbol{\sigma}])^2 \quad (14)$$

$$I_3 = \mathrm{Tr}[\boldsymbol{\sigma}] - \mathrm{Tr}[\mathbf{A} \cdot \boldsymbol{\sigma}] \quad (15)$$

The four parameters $\varsigma_i (i = 1,4)$, and their corresponding invariants represent different loading states. The first parameter ς_1 is related to transverse shear loading, while ς_2 accounts for the material performance under in-plane shear loading. The parameters ς_3 and ς_4 regard loading conditions transverse to the fiber direction.

A schematic representation of the yield surface in the invariant space is portrayed in Figure 2.

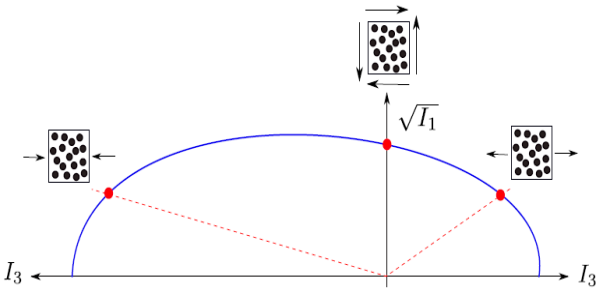

Figure 2: Schematic illustration of the yield surface in the invariant space.

In line with [5], a non-associative flow rule is introduced in the present model, i.e. the evolution of the plastic strains is not governed by the gradient of the yield function. Accordingly, a plastic potential function $\mathcal{G}(\boldsymbol{\sigma}, \mathbf{A}, \bar{\boldsymbol{\varepsilon}}^p)$ is introduced. By omitting the linear term associated with I_3 from the definition of the yield function, the plastic flow function is defined as follows:

$$\mathcal{G}(\boldsymbol{\sigma}, \mathbf{A}, \bar{\boldsymbol{\varepsilon}}^p) = \iota_1 I_1 + \iota_2 I_2 + \iota_3 {I_3}^2 \leq 0 \quad (16)$$

where $\iota_i (i = 1,3)$ are the set of plastic potential parameters.

3.4 Internal Variables Evolution Equations

The evolution equations of the internal variables, namely the plastic strains $\boldsymbol{\varepsilon}^p$ and the hardening variables $\boldsymbol{\xi}$, are expressed by the following rates:

$$\dot{\boldsymbol{\varepsilon}}^p = \gamma \, \partial \mathcal{G} / \partial \boldsymbol{\sigma} \, ; \; \dot{\boldsymbol{\xi}} = \partial \mathcal{G} / \partial \boldsymbol{\Gamma} \quad (17)$$

where γ refers to so-called plastic multiplier.

The customary loading/unloading conditions according to Kuhn-Tucker are expressed as:

$$\gamma \geq 0; \; \mathcal{F}(\boldsymbol{\sigma}, \mathbf{A}, \bar{\boldsymbol{\varepsilon}}^p) \leq 0; \; \gamma \mathcal{F}(\boldsymbol{\sigma}, \mathbf{A}, \bar{\boldsymbol{\varepsilon}}^p) = 0 \quad (18)$$

Moreover, the consistency condition renders:

$$\gamma \dot{\mathcal{F}}(\boldsymbol{\sigma}, \mathbf{A}, \bar{\boldsymbol{\varepsilon}}^p) = 0 \quad (19)$$

3.5 Parameters Identification

To determine the four yield surface parameters $\varsigma_i (i = 1,4)$, for each of the triggering points of the yield locus shown in Figure 2, the yield stress vs. the corresponding plastic strain has to be obtained. Based on the yield function definition, Eq. (12), the following yield stresses are necessary to fully identify the yield surface: (i) uniaxial transverse tensile yield stress ${\sigma^y}_{utt}({\varepsilon^p}_{utt})$, (ii) uniaxial transverse compressive yield stress ${\sigma^y}_{uct}({\varepsilon^p}_{uct})$, (iii) in-plane shear yield stress ${\sigma^y}_{is}({\varepsilon^p}_{is})$, and (iv) transverse shear yield stress ${\sigma^y}_{ts}({\varepsilon^p}_{ts})$.

The purpose behind the introduction of a non-associative flow rule is the determination of a realistic plastic deformation behavior, particularly in terms of the so-called plastic Poisson coefficients. Accordingly, the plastic potential parameters $\iota_i (i = 1,3)$ are explicitly represented in terms of plastic Poisson coefficients, see [5].

3.6 Numerical Treatment

The numerical scheme for the solution of the initial boundary value problem (IBVP) associated with the present problem is constructed in two principal steps: (i) the local (point) integration of the model utilizing an appropriate return mapping algorithm, (ii) the employment of the result arises from the previous step in the constitutive block of the weak formulation of the problem, which is discretized in space by means of finite element method and solved using the standard incremental-iterative Newton-Rahpson scheme.

Locally, for the local integration of the local initial boundary value problem (IBVP), the backward Euler procedure is employed to trigger the update of the internal variables of the constitutive model. Herein, the so-called operator split (predictor-corrector) with a general return mapping is used as a solution process.

Globally, using an implicit FE formulation, the computation of the algorithmic consistent tangent moduli, guarantees the quadratic convergence along the incremental-iterative solution process.

The thorough presentation of the numerical treatment is omitted here for the sake of the conciseness. For a detailed description, the reader is referred to [5].

4 Applications

The constitutive formulation previously described is implemented into the commercial FE code Abaqus/Standard by means of the user-defined capabilities UMAT for the geometrically nonlinear analyses of FRP composites. The goal of this section is to discuss the implementation of the model and thereafter to assess the performance of the proposed formulation.

4.1 Implementation in Abaqus/Standard

During the global computation, the user subroutine UMAT is called at all material calculation points of elements for which the material definition includes a user-defined material behavior. Besides updating the stresses and solution-dependent state variables at the end of the increment, the subroutine must also provide the material Jacobian matrix, for the mechanical constitutive model, see [7].

The incremental strains in the rotated frame are passed in by the UMAT. The total strains are also given. However, their components are rotated to account for rigid body motion in the increment before UMAT is called.

The total strains, as well as the stresses at the beginning of the increment, are passed in. Before the UMAT routine is called, the components of these quantities are rotated to account for rigid body motion in the increment. However, the stresses must be updated in this routine to be the stress tensor at the end of the increment.

One major concern is the solution-dependent state variables. These variables are also passed in as the values at the beginning of the increment. However, to account for rigid body motion of the material, the vector-valued or tensor-valued state variables must be rotated. For this purpose, the rotation increment matrix (the increment of rigid body rotation of the element local co-rotational coordinate system) is provided so that vector- or tensor-valued state variables can be rotated appropriately in this subroutine. Thereafter, the state variables must be updated based on the constitutive behavior.

4.2 Model Verification and Validation: Transverse Uniaxial Tension and Compression

The first application concerns the simulation of the transverse uniaxial tension compression of a Hex-Ply IM7-8552 UD carbon epoxy presented. For this purpose, a cube specimen with dimensions of $1 \times 1 \times 1\ \mathrm{mm}^3$ is used. The objective of this first example is the verification of the current formulation for its subsequent application in a more complex structural example.

The material data (elastic and plastic properties) needed for the model calibration are taken from [8,9]. The elastic material properties are reported in Table 1. The plastic material properties are not provided here for the sake of the conciseness.

Table 1. IM7-8552: elastic properties

E_{11}(MPa)	E_{22}(MPa)	G_{12}(MPa)	ν_{12}	ν_{23}
181500.43	9900.86	6160.76	0.0185	0.38

For both, uniaxial tension and compression, the specimen is discretized by 25 elements. The 8-node linear brick element type C3D8 is used for the discretization. The boundary conditions imposed onto the FE model replicates those for uniaxial stress states, see Figure 3.

Figure 4 reports the experimental-numerical correlations. In this graph, an excellent agreement between the experimental data and the numerical predictions can be observed.

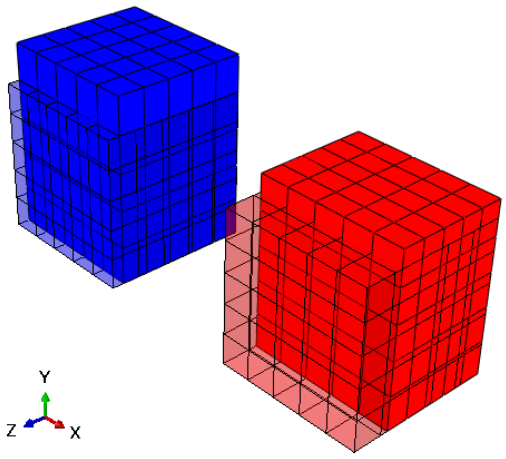

Figure 3: FE-discretization and undeformed/ deformed configuration: uniaxial transverse tension in Y direction (blue) and transverse compression in Z direction (red).

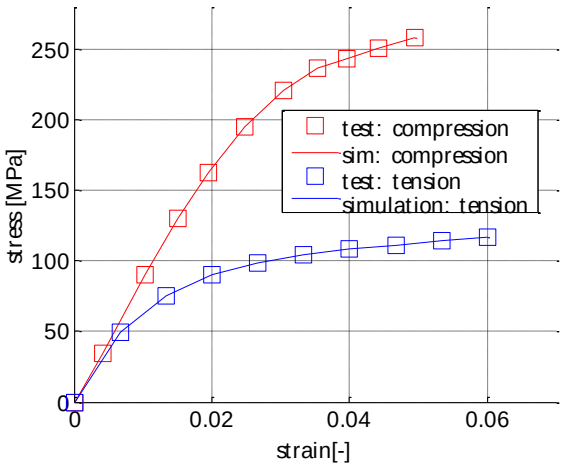

Figure 4: Experimental numerical correlation of unidirectional carbon-epoxy IM7-8552 under transverse loading: tension (blue) and compression (red).

4.3 Structural Application: 3-Point Bending

Now the 3-point bending of a UD FRP plate manufactured from IM7-8552 is considered.

The geometric description of the plate is given in Figure 5. The dimensions of the plate are: (i) length L = 60 mm, (ii) width B = 8 mm, and (iii) thickness t = 2 mm.

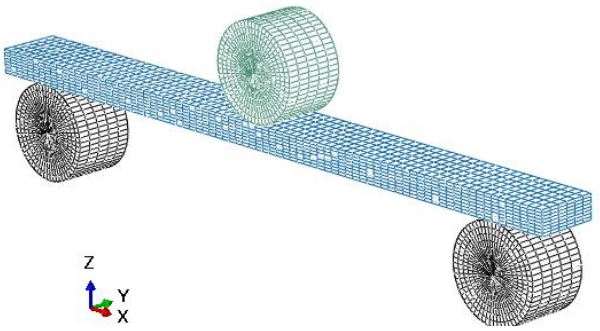

Figure 5: 3-point bending of a UD FRP plate: FE-discretization.

After a mesh convergence study, the numerical model consists of the discretization of the FRP plate using 3840 elements, whereas the pin for the loading application and support is meshed using 2100 elements. The plate is considered deformable, accordingly, the brick element type C3D8 is used for the discretization. The pin part is assumed to be discrete rigid body and the bilinear rigid quadrilateral element type R3D4 is employed.

For the contact interaction between the rigid bodies and the plate, the balanced master-slave general contact algorithm is utilized for its ease.

The external loading is applied through a prescribed vertical displacement downwards at the central pin equal to 4 mm.

Figure 6 depicts the fiber orientation (material orientation) before the computation. The change in orientation predicted by the current model at the end of the simulation is shown in Figure 7. In this graph, a change of the material direction throughout the loading process is observed. This change is taking place due to the large rotations and displacements experienced by the UD sheet, which cannot be predicted using a geometrically linear constitutive model.

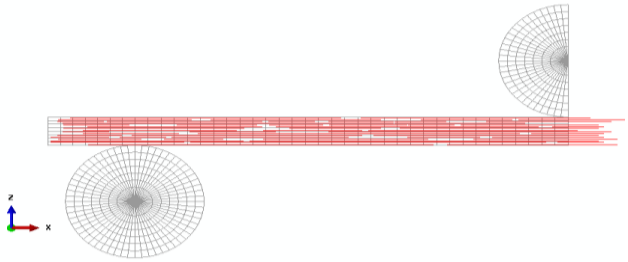

Figure 6: 3-point bending of a UD FRP plate: Mapping of the fiber direction (red) before the computation.

This becomes evident in the current example and highlights the necessity of triggering the evolution of the material (fiber) orientation along the loading and deformation process. This issue can be only performed using a geometrically nonlinear setting.

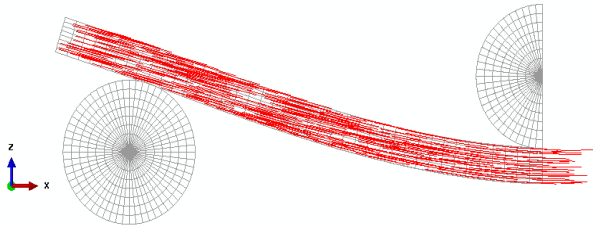

Figure 7: 3-point bending of a UD FRP plate: Mapping of the fiber direction (red) after the computation.

Moreover, Figure 8 shows the stress distribution along the plate.

5 Conclusion

In this paper, a co-rotational formulation of an invariant-based anisotropic plasticity model including aspects of its numerical treatment and implementation within the FE framework has been presented for geometrically nonlinear analyses of composites.

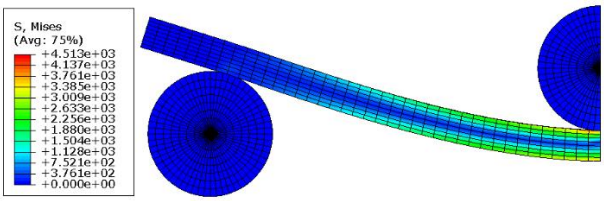

Figure 8: 3-point bending of a UD FRP plate: von Mises stress distribution.

The proposed formulation assumed a pressure dependent yield surface and a non-associate flow rule to capture realistic evolution of the inelastic behavior.

The model is then employed in a co-rotational framework so that geometrically non-linear effects can be captured. On the computational side, important aspects regarding the numerical treatment and implementation of the proposed formulation in Abaqus/Standard are discussed.

Finally, the performance of the current model has been verified and validated through the simulation of uniaxial stress states in a UD FRP composites. Subsequently, the model has been incorporated into the simulation of a 3-point bending problem. One key aspect regarded the possibility of triggering the preferential material orientation along the deformation process.

The upcoming focus regards the employment of the model in the simulation of practical applications of FRP

composites where geometrical nonlinear effects play an important role.

Acknowledgments

This paper is dedicated to the memory of Dr. Matthias Vogler, an exceptional young scientist that sadly left us too soon. Many thanks and gratitude also goes to Nabeel Safdar and Yaqin Ali for the helpful comments and discussions.

References

[1] Zoghi M. *The International Handbook of FRP Composites in Civil Engineering*. Boca Raton, Florida: CRC Press Inc, 2013.

[2] Kanouté P, Boso DP, Chaboche JL, et al. Multiscale Methods for Composites: A Review. *Arch Computat Methods Eng* 2009; 16: 31–75.

[3] Hine PJ, Rudolf Lusti H, Gusev AA. Numerical simulation of the effects of volume fraction, aspect ratio and fibre length distribution on the elastic and thermoelastic properties of short fibre composites. *Composites Science and Technology* 2002; 62: 1445–1453.

[4] Hackl K, Miehe C, Celigoj C. Theory and numerics of anisotropic materials at finite strains (EUROMECH Colloquium 394). *International Journal of Solids and Structures* 2001; 38: 9421.

[5] Dean A. *Material Modeling of Short Fiber Reinforced Polymeric Composites: Theory, Numerical Aspects, and Applications*. Gottfried Wilhelm Leibniz Universität Hannover, 2017.

[6] Masud A, Tham CL. Three-Dimensional Corotational Framework for Elasto-Plastic Analysis of Multilayered Composite Shells. *AIAA Journal* 2000; 38: 2320–2327.

[7] *ABAQUS/CAE User's Manual*. Hibbitt, Karlsson & Sorensen, Incorporated, 2002.

[8] Koerber H, Xavier J, Camanho PP. High strain rate characterisation of unidirectional carbon-epoxy IM7-8552 in transverse compression and in-plane shear using digital image correlation. *Mechanics of Materials* 2010; 42: 1004–1019.

[9] Vogler M, Rolfes R, Camanho PP. Modeling the inelastic deformation and fracture of polymer composites – Part I: Plasticity model. *Mechanics of Materials* 2013; 59: 50–64.